12-1-2012

miR-786 Regulation of a Fatty-Acid Elongase Contributes to Rhythmic Calcium-Wave Initiation in *C. elegans*

Benedict J. Kemp
Marquette University

Erik Allman
University of Rochester

Lois Immerman
Oberlin College

Megan Mohnen
Marquette University

Maureen A. Peters
Oberlin College

See next page for additional authors

Accepted version. *Current Biology*, Vol. 22, No. 23 (December 2012): 2213–2220. DOI.

Authors
Benedict J. Kemp, Erik Allman, Lois Immerman, Megan Mohnen, Maureen A. Peters, Keith Nerhke, and Allison Abbott

Title:
miR-786 regulation of a fatty acid elongase contributes to rhythmic calcium wave initiation in *C. elegans*

Authors:
Benedict J. Kemp[1], Erik Allman[2], Lois Immerman[3], Megan Mohnen[1], Maureen A. Peters[3], Keith Nehrke[4], and Allison L. Abbott[1,*]

[1]Department of Biological Sciences
Marquette University
Milwaukee, Wisconsin 53201

[2] Department of Pharmacology and Physiology
University of Rochester School of Medicine and Dentistry
Rochester, New York

[3]Department of Biology
Oberlin College
Oberlin, Ohio 44074

[4]Department of Medicine
University of Rochester School of Medicine and Dentistry
Rochester, New York

*Correspondence: allison.abbott@marquette.edu

running title (50 characters max): *mir-786* regulates rhythmic calcium waves

Summary

Background: Rhythmic behaviors are ubiquitous phenomena in animals. In *C. elegans,* defecation is an ultradian rhythmic behavior: every ~50 s a calcium wave initiating in the posterior intestinal cells triggers the defecation motor program (DMP) that comprises three sequential muscle contractions. Oscillatory calcium signaling is central to the periodicity of defecation. The posterior-most intestinal cells function as the pacemaker for this rhythmic behavior, although it is unclear how the supremacy of these cells for calcium wave initiation is controlled.
Results: We describe how the loss of the *mir-240/786* microRNA (miRNA) cluster, which results in arrhythmic defecation, causes ectopic intestinal calcium wave initiation. *mir-240/786* expression in the intestine is restricted to the posterior cells that function as the defecation pacemaker. Genetic data indicate that *mir-240/786* functions upstream of the inositol 1,4,5-trisphosphate (IP_3) receptor. Through rescue analysis, it was determined that miR-786 functions to regulate defecation. Furthermore, we identified *elo-2*, a fatty acid elongase with a known role in defecation cycling, as a direct target for miR-786 and that regulation of palmitate levels by *elo-2* is the likely mechanistic link to defecation.
Conclusions: Together, these data indicate that miR-786 confers pacemaker status on posterior intestinal cells for the control of calcium wave initiation through the regulation of *elo-2* and subsequently palmitate levels. We propose that a difference in fatty acid composition in the posterior intestinal cells may alter the activities of membrane proteins, such as IP_3 receptor or TRPM channels, that control pacemaker activity in the *C. elegans* intestine.

Highlights

- *mir-240/786* acts upstream of IP_3 receptor activity to regulate defecation
- Loss of *mir-240/786* results in ectopic calcium wave initiation in the intestine
- The fatty acid elongase *elo-2* is a likely direct target of miR-786
- *mir-240/786* functions in the posterior intestine to confer pacemaker activity

Introduction

Biological rhythms range from the annual migratory behaviors of animals, to the circadian regulation of physiological pathways, to the ultradian rhythms of the heart. Many ultradian rhythms, which have cycles of less than a day, are controlled by oscillations of intracellular calcium. Signals from pacemaker cells drive changes in intracellular calcium levels that initiate and coordinate contractions of the heart as well as of smooth muscle tissues, such as the gut [1-4]. Three rhythmic behaviors have been described in *C. elegans*: pharyngeal peristalsis [5], gonadal sheath contractions [6], and defecation [7]. *C. elegans* has been used extensively to study oscillatory calcium signaling and rhythmic behaviors [reviewed in 8].

The defecation motor program (DMP) is a rhythmic behavior that occurs every ~50 s and comprises three stereotypical contractions: a posterior body wall muscle contraction, an anterior contraction, and an enteric muscle contraction followed by expulsion. The posterior body contraction step is initiated by a calcium elevation in the posterior intestine, which requires IP_3 receptor-mediated release from intracellular calcium stores [9-11] along with an influx of extracellular calcium through the TRPM channels, GON-2 and GTL-1 [12-14]. These calcium elevations lead to the extrusion of protons from the intestine to the pseudocoelomic space via PBO-4/NHX-7 sodium-proton exchanger activity. Pseudocoelomic acidification then triggers the contraction of the posterior body wall muscle [15, 16].

The posterior intestine functions as the pacemaker in the initiation and coordination of the DMP [7]. The nematode intestine is a single-cell layer tube of 20 polarized epithelial cells that are joined by gap junctions and are organized into nine intestinal rings from the anterior int1to the posterior int9 [17, 18]. Calcium release in the posterior intestine triggers an anterior-directed intercellular calcium wave throughout the intestine, which is essential for normal execution of the DMP [18, 19]. Hence, cells of the posterior intestinal ring are the site of the behavioral pacemaker [7].

The molecular mechanisms that confer pacemaker activity to the posterior intestine are largely unknown. Pacemaker activity for calcium wave initiation is an intrinsic property of intestinal cells since rhythmic calcium waves persist in isolated intestines [10]. Because all intestinal cells are capable of initiating calcium waves [18, 19], pacemaker activity likely involves establishing a different threshold for intracellular calcium release in the posterior intestine relative to neighboring intestinal cells. Therefore, differences in the expression or activity of critical regulators of calcium sensitivity must exist in the posterior intestine.

microRNAs (miRNAs) are ~22nt non-coding small RNAs that post-transcriptionally repress translation of downstream target mRNAs [20, 21]. Interestingly, analysis of miRNA deletion mutants identified a miRNA cluster, *mir-240/786*, that functions to regulate defecation cycling. The loss of *mir-240/786* results in long and

arrhythmic defecation cycles [22]. Here we show that *mir-240/786* is expressed in the posterior-most int9 cells. We demonstrate that *mir-240/786* mutants display defects in calcium wave initiation in the posterior intestine. Rescue experiments demonstrate that *mir-786*, not *mir-240*, activity is required for normal defecation cycling. Furthermore, we have identified *elo-2*, which encodes a fatty acid elongase, previously implicated in defecation behavior [23], as a direct target of miR-786. Our results suggest that miR-786 acts cell-autonomously to ensure calcium wave initiation in the posterior intestinal cells by regulating fatty acid composition through repression of *elo-2*.

Results

miR-786 functions to regulate defecation

mir-240 and *mir-786* are miRNA genes that are conserved in many species including humans, where the related miRNA genes are *mir-193b* and *mir-365a*, respectively (Figure 1A). The sequences encoding these two miRNAs are located in a genomic cluster (Figure 1B). We first determined which miRNA in this cluster functions to regulate defection. We performed rescue analysis with genomic fragments that were mutated to delete the 22 nucleotide sequence coding for miR-240, miR-786, or both. Defecation defects were rescued with genomic fragments containing *mir-786* but not *mir-240* (Figure 1, Table S1). These results indicate that *mir-786* is necessary for rhythmic defecation cycling in worms.

mir-240/786 is expressed in the intestine and somatic gonad.

Previously, *mir-240/786* expression was observed in the uterus, spermatheca, and gonadal sheath cells beginning in the L3 stage [24]. Since loss of *mir-240/786* causes defecation arrhythmia [22], we performed further analysis of *mir-240/786* expression to determine if *mir-240/786* was expressed in cells required for defecation, such as the intestine, body wall muscle, enteric muscle, or the AVL/DVB neurons [25]. We observed consistent GFP expression in the posterior-most int9 intestinal cells (Figure 1C and 1E)[17]. Weaker expression was observed with lower penetrance in the four cells of the anterior-most int1 intestinal cells (Figure 1D). No expression was observed in the body wall muscle, enteric muscle or neurons.

Loss of *mir-240/786* results in defects in the initiation of the DMP.

Consistent with earlier observations [22], we found that *mir-240/786* worms display long, arrhythmic defecation cycles as determined by the length of time between consecutive posterior body contraction events (Figure 2). While average defecation cycle periodicity was consistently longer than in wild-type worms, there was variability in the extent of arrhythmia observed between individual *mir-240/786* mutant worms (Figure 2B and 2C). *mir-240/786* worms displayed additional defects in defecation behavior. First, in contrast to the smooth, rapid posterior contraction in wild-type worms (Movie S1), the posterior contraction in *mir-240/786* mutants often appeared to be biphasic, with an initial weak contraction, followed by a full contraction (Movie S1). This was associated with a longer interval between the posterior contraction and subsequent steps in the motor program: on average in wild-type worms an expulsion occurred 4.3 $\pm$ 0.5 s after a posterior contraction, while in *mir-240/786* worms this increased to 5.5 $\pm$ 1.9 s. Second, weak

posterior contractions that were not associated with a full DMP occurred in 34.6% of the defecation cycles (Movie S1). Finally, *mir-240/786* worms failed to execute an enteric muscle contraction and expulsion following a strong posterior body contraction event in 14.8% of the cycles (Movie S1).

***mir-240/786* functions upstream of IP_3 receptor-mediated calcium release.**

IP_3 receptor-mediated calcium release in the intestine is an essential regulator of defecation cycling in worms (Figure 3A). The level of IP_3 receptor activity can determine the length of the defecation cycle: worms with reduced activity of *itr-1,* which encodes the IP_3 receptor in worms, display long defecation cycles whereas worms that overexpress *itr-1(+)* show short defecation cycles [9]. We found the long defecation phenotype associated with the *itr-1(sa73)* mutant was enhanced in *itr-1(sa73)*; *mir-240/786* double mutant worms, with some worms failing to show any posterior body contractions during 10 minutes of monitoring (data not shown).

In order to determine whether *mir-240/786* functioned upstream of *itr-1*, we performed epistasis analysis with gain-of-function alleles of *itr-1*. There are multiple gain-of-function *itr-1* mutations, including the *sy290* allele, which is predicted to enhance IP_3 binding affinity approximately two fold [26], and the *sy327* allele, which affects the calcium binding domain [10]. These mutations have been shown to suppress the long defecation cycle phenotypes caused by mutations in upstream signaling processes, such as loss of *plc-3,* which encodes phospholipase Cγ [10]. We found that both the *sy290* and *sy327 itr-1* gain-of-function alleles were able to suppress the defecation defects associated with the loss of *mir-240/786* (Figure 3B).

We next determined whether mutations that result in enhanced levels of IP_3 could also suppress the defecation cycle defects in *mir-240/786* mutants. Loss of either IP_3 kinase (*lfe-2)* or IP_3 phosphatase (*ipp-5)* activities are expected to result in elevated levels of IP_3, due to reduced conversion of IP_3 into IP_4 or IP_2 (Figure 3A). Like *itr-1* gain-of-function alleles, loss of *lfe-2* or *ipp-5* suppresses defecation defects associated with mutations in upstream signaling processes. We found that loss of *lfe-2* or *ipp-5* was able to suppress the *mir-240/786* defecation defects (Figure 3B). Taken together, these data indicate that *mir-240/786* functions upstream or in parallel to IP_3 receptor activity in the regulation of the DMP.

***mir-240/786* is necessary for stereotypical calcium wave initiation and confers pacemaker cell status.**

Given the central role of the IP_3 receptor in calcium signaling in the *C. elegans* intestine, we next determined how the loss of *mir-240/786* influenced calcium oscillations and calcium wave propagation during defecation. Live, freely-moving animals expressing the calcium biosensor D3cpV [27] in the intestinal cytoplasm were used for dynamic fluorescent imaging to measure the relative change in cytoplasmic calcium throughout the entire intestine in wild-type and *mir-240/786* mutant worms. Representative calcium oscillations are shown in Figures 4A, 4C, and Movie S2. In wild-type worms, each calcium peak represents a fast intercellular calcium wave that initiates in the posterior intestine and propagates anteriorly (Movie S2) [10, 11, 19].

Multiple defects in calcium oscillations were observed in *mir-240/786* mutants. First, calcium oscillations were arrhythmic and differed greatly in magnitude in *mir-*

240/786 mutants (Figure 4C) relative to wild-type controls (Figure 4A). Second, multiple calcium events occurred in each defecation cycle (Figure 4H), with small calcium increases often preceding successively larger calcium increases, until the DMP was triggered (Figure 4C, S1). Third, the spatial pattern of calcium wave initiation was strikingly altered in *mir-240/786* mutants. Whereas in wild-type worms, calcium wave initiation is restricted to the anterior and posterior ends of the intestine [19], calcium wave initiation in *mir-240/786* mutants often occurred at ectopic sites in internal intestinal cells (Figure 4G, Movie S2). These ectopic calcium elevations occasionally resulted in both forward and reverse waves (Figures 4E and S1, Movie S2). However, ectopic calcium waves were often insufficient to elicit a large calcium release in posterior intestinal cells, which is necessary to trigger a posterior body contraction. Thus, in *mir-240/786* mutants, the posterior intestine appears refractory to robust calcium release and wave initiation. Consistent with our behavioral data, we found that the *sy327* gain of function allele of *itr-1* was able to fully suppress the arrhythmic calcium oscillations and ectopic calcium wave initiation associated with loss of *mir-240/786* (Figure S2), suggesting that *mir-240/786* acts upstream of the IP_3 receptor to regulate calcium signaling.

Acidification of the intestinal cytoplasm results from calcium signaling during defecation and contributes to the behavioral output [16]. Consistent with *mir-240/786* acting upstream of the IP_3 receptor, acidification events were arrhythmic in *mir-240/786* worms (Figure 4B and 4D). Individual acidification events looked largely similar to wild-type, although unlike in wild-type worms, low amplitude changes in the cytoplasmic pH in the posterior intestinal cells were observed in *mir-240/786* mutants. These low amplitude pH changes correlated with the observed small calcium elevations and weak posterior contractions (Figure 4F, S1). It is likely that calcium must be elevated over a threshold level to trigger robust acidification and full posterior body contraction. Collectively, these data indicate that *mir-240/786* functions upstream of IP_3 receptor activity to promote calcium elevation and wave initiation in the posterior intestine.

Identification of *elo-2* as a target of miR-786 in the posterior intestine

In order to identify relevant miR-786 targets, we tested computationally-predicted targets using RNAi. Typically, miRNAs repress the translation of target mRNAs through imperfect binding to sites in target 3' UTRs [20]. Thus, the phenotype of *mir-240/786* mutant worms results from elevated levels of miR-786 targets. Candidate targets were identified using mirWIP [28], PITA [29], and Targetscan 5.1 [30, 31]. Of the candidates tested, only knockdown of *elo-2* resulted in a near complete suppression of the long defecation cycle periodicity in *mir-240/786* worms (Figure 5A, Table S2). *elo-2(RNAi)* also suppressed the weak posterior contractions observed in *mir-240/786* mutants (data not shown). *elo-2* encodes a fatty acid elongase, which has been shown to regulate defecation cycling [23], and has a single predicted miR-786 binding site in its 3' UTR (Figure 5B). Knockdown of *elo-2* in wild-type worms alters levels of fatty acids, with a significant increase observed in the level of palmitate (C16:0) [23]. Interestingly, higher levels of *elo-2* specifically in the posterior intestine extended the defecation period [23], similar to the phenotype observed in *mir-240/786* worms.

mir-240/786; elo-2(RNAi) worms had a shorter average defecation period but still had a higher coefficient of variation (13.8% CV) in the lengths of defecation cycles

compared to *elo-2(RNAi)* worms (4.1% CV, Table S2). Calcium imaging of these worms showed that the arrhythmia of calcium oscillations was largely suppressed in *mir-240/786;elo-2(RNAi)*, but surprisingly, knockdown of *elo-2* did not restore calcium wave initiation to the posterior intestine in *mir-240/786* mutants (Figures 5C and 5D). Instead, these worms showed predominantly anterior initiated calcium waves, which subsequently triggered a posterior calcium wave and a DMP. This is consistent with the idea that reducing *elo-2* expression amplifies calcium signaling, but that the supremacy of the pacemaker is determined by the difference in *elo-2* expression level relative to other cells. Knockdown of *elo-2* in wild-type worms resulted in fast posterior-initiated calcium waves, suggesting that either an *elo-2* gradient persists following knockdown or that there are other mechanisms that help to establish pacemaker supremacy in addition to *elo-2* expression levels.

To test whether *elo-2* is a direct target of miR-786, we first analyzed *elo-2* mRNA levels. A modest increase was observed in *elo-2* mRNA levels in *mir-240/786* worms relative to wild-type worms (Figure S3). In order to determine if *elo-2* is regulated specifically in the posterior intestine, we analyzed the expression of *gfp* under the control of the *elo-2* 5' promoter and either the *elo-2* 3' UTR or a mutated *elo-2* 3' UTR in which the miR-786 putative binding site was deleted. An *elo-2*^{prom}*::gfp* reporter under the control of the *unc-54* 3' UTR is expressed uniformly throughout the intestine [23]. However, a different expression pattern was observed in worms expressing *elo-2*^{prom}*::gfp::elo-2*$^{3'\ UTR}$, which showed little GFP expression in the int9 posterior intestinal cells relative to the neighboring int8 cells in most wild-type worms (Figure 5E and 5F). Loss of *mir-240/786* resulted in fewer worms that displayed this int9 specific repression of GFP (Figure 5G). For 3/5 transgenic lines, this pattern of reduced GFP expression in int9 posterior cells is significantly altered in *mir-240/786* mutant worms.

Deletion of the putative miR-786 binding site from the *elo-2* 3' UTR resulted in weaker repression of GFP levels in the posterior intestine. Fewer worms expressing *elo-2*^{prom}*::gfp::elo-2*$^{3'\ UTRmut}$ showed low GFP expression in int9 relative to int8. No difference was observed between wild-type and *mir-240/786* mutants for 5/5 transgenic lines (Figure 5G). These data indicate that *elo-2* repression in int9 posterior cells requires the miR-786 binding site in the *elo-2* 3' UTR and that *elo-2* is likely a direct target of miR-786 in the int9 posterior cells.

Knockdown of *elo-2* results in elevated levels of palmitate, which is sufficient to cause short defecation cycles in wild-type worms [23]. Therefore, we tested the hypothesis that the long arrhythmic defecation cycles in *mir-240/786* result from reduced palmitate levels caused by elevated *elo-2* activity. To test this, wild-type and *mir-240/786* worms were grown on plates supplemented with palmitate. Palmitate supplementation was sufficient to suppress the long arrhythmic defecation cycles in *mir-240/786* mutant worms, though wild-type worms did not show shorter defecation cycles in these experiments (Figure 5H). These data suggest that the *mir-240/786* defecation defects results from reduced palmitate levels in the posterior intestine, possibly by altering protein palmitoylation of regulatory membrane proteins or the lipid composition of cell membranes (Figure 5I).

Discussion

Defecation in wild-type worms is a stereotypical rhythmic behavior with a cycle period of ~50 s [25]. While calcium signaling in the intestine is central for this periodicity, the pacemaker mechanism that spatially constrains calcium wave initiation is not understood. In this work, we have identified a miRNA cluster, *mir-240/786,* that is expressed in the posterior-most intestinal cells and is required for the rhythmic initiation of forward calcium waves. Our genetic and calcium imaging data indicate that *mir-240/786* functions upstream of IP_3 receptor activity to regulate calcium oscillations through the regulation of *elo-2*. Rescue experiments showed that *mir-786,* but not *mir-240,* is necessary for normal defecation cycling. miR-786 may function to either amplify the pacemaker signal that triggers calcium elevation or, alternatively, lower the threshold for calcium elevation in response to the pacemaker signal. Hence, by virtue of its expression pattern, *mir-786* can contribute to establishing or maintaining the supremacy of the posterior intestinal cells as the defecation pacemaker through the repression of *elo-2* and subsequent regulation of fatty acid composition in the posterior intestine.

mir-240/786 mutants have defects in calcium elevation and wave initiation in the posterior intestine. In wild-type worms, calcium waves are initiated rhythmically in the posterior intestine. In contrast, in *mir-240/786* mutant worms, sites of calcium wave initiation appear to be stochastic, with only ~20% of calcium waves initiating from the posterior intestine. Similar ectopic calcium waves occur in *inx-16* mutants, which lack a pannexin gap junction protein [18] and *egl-8* mutants, which lack PLCβ activity [19]. It is likely that *inx-16* functions to maintain the supremacy of the posterior intestine by facilitating the forward propagation of calcium waves from the posterior intestine. The PLCβ protein, EGL-8, is enriched at points of cell-cell contact in the posterior intestine [32, 33] and may act to amplify and propagate forward calcium waves.

The observed defects in calcium oscillations and wave initiation can account for the defecation defects in *mir-240/786* mutants. First, *mir-240/786* mutants display arrhythmic posterior body contractions that correspond to the arrhythmic calcium oscillations. Second, we observed a biphasic execution of the posterior body contraction, with a weak partial contraction that immediately precedes a full contraction. This likely reflects minor calcium events that occur prior to a large magnitude calcium release, which is sufficient to trigger robust acidification and a full posterior body contraction. In contrast, weak contractions were associated with slight pseudocoelomic acidification. Third, *mir-240/786* mutants had weak posterior contractions in the middle of defecation cycles, which are also likely due to the observed low magnitude calcium events that fail to trigger robust acidification and a full contraction. Finally, we observed posterior body contractions that were not followed by an expulsion, which may result from calcium events in posterior cells that fail to propagate a forward calcium wave.

Our data suggests that posterior cells in *mir-240/786* mutants have reduced ability to either generate or respond to the pacemaker signal for calcium release relative to wild-type worms. While we cannot strictly rule out a developmental effect of mir-240/786 on intestinal physiology, it appears more likely that the miRNA participates in the oscillatory calcium signaling process. The pacemaker signal that initiates calcium release is unknown but may be calcium itself or IP_3 [14]. While miR-786 is necessary to establish or maintain the supremacy of the posterior intestine in the initiation of calcium waves and control of defecation cycling, it is likely not the only regulator that acts to ensure the supremacy of the posterior intestine. Rhythmic defecation and calcium wave

initiation from the posterior intestine is observed in the absence of *mir-240/786* when the activity of the IP_3 receptor is elevated, through a gain of function mutation. This suggests that additional regulatory factors in the posterior intestine function downstream of IP_3 receptor-dependent calcium release to maintain the rhythmicity of defecation cycling. One such regulator may be EGL-8, which is localized in the posterior intestine and is required to ensure the rhythmic initiation of calcium waves from the posterior intestine [19].

miR-786 regulates defecation in part through the repression of *elo-2* in the posterior-most intestinal cells. *elo-2* is transcribed uniformly throughout the intestine [23]. Our data indicate that *elo-2* is repressed by miR-786 in the posterior intestine, predicted to result in lower ELO-2 protein levels in int9 relative to neighboring cells. Our data indicate that miR-786 directly represses *elo-2* through the single predicted binding site in the *elo-2* 3' UTR. Since some repression of *gfp* expression is observed in the absence of miR-786 and in the absence of the miR-786 binding site, it is likely that additional miRNAs or proteins function to regulate *elo-2* levels in the posterior intestine. A single binding site is expected to mediate modest repression [20], though the extent of repression depends upon the relative levels of miR-786 and *elo-2* mRNA [34]. Our expression analysis of reporter transgenes is consistent with a modest level of repression by miR-786. It remains possible that miR-786 functions to regulate additional targets, which were not tested in this study.

miR-786 repression of *elo-2* is expected to alter the fatty acid composition in the posterior-most intestinal cells. Reduced *elo-2* activity results in significantly elevated palmitate levels [23]. Interestingly, palmitate supplementation is sufficient to cause faster defecation cycles in wild-type worms [23] and to suppress the long arrhythmic defecation cycles in *mir-240/786* mutant worms. Therefore, miR-786 repression of *elo-2* activity in the posterior intestine may promote higher palmitate levels, which may enhance palmitoylation of key regulatory membrane proteins. Protein palmitoylation is a reversible modification and thus can provide dynamic regulation of the localization and activity of membrane proteins, including ion channels [35, 36]. Enhanced palmitoylation in the posterior intestine may sensitize these cells to promote faster calcium oscillations relative to the neighboring cells in the intestine.

One model to account for the intrinsic oscillating activity of calcium release involves the periodic entry of extracellular calcium. A small amount of calcium entry may be sufficient to either activate ITR-1 directly or to activate PLCγ activity, which produces IP_3 and triggers calcium release from the ER. Activation of PLCγ also lowers PIP_2 levels, which relieves the inhibition of TRPM calcium channels, GON-2/GTL-1, at the plasma membrane [13, 14]. Calcium flux through both GON-2/GTL-1 TRPM channels and ITR-1 IP_3 receptor channels contributes to robust cytoplasmic calcium elevation [9-11, 13]. We speculate that miR-786 repression of ELO-2 levels in the posterior intestinal cells establishes differences in the levels of fatty acids, such as palmitate, that could modulate the activity of membrane proteins, which control calcium signaling. Candidate membrane proteins that may be regulated by palmitoylation include the GON-2/GTL-1 TRPM channels, the ITR-1 IP_3 receptor, and KQT-2/3 KCNQ potassium channels, which contain putative palmitoylation sites identified using the CSS-Palm 3.0 prediction algorithm [37]. Increased palmitoylation may lower the threshold for calcium elevation in the int9 posterior-most cells and thereby ensure faster calcium

oscillations and reliable calcium wave initiation from these cells. Alternatively, differences in lipid composition of the membranes in the posterior intestine may promote targeting regulatory proteins to the plasma membrane that may act to regulate calcium release.

Experimental Procedures

General Procedures

C. elegans strains were maintained at 20˚C on *Escherichia coli* strain AMA1004 under standard conditions. Strains used are listed in Supplemental Table 2. The Supplemental Experimental Procedures contains detailed information on strain and plasmid construction, microscopy, calcium and pH imaging, RNAi, qPCR, and fatty acid supplements.

Defecation Assays

For wild-type and mutant strains, young adult worms (within 24 hrs of the L4 molt) were scored at room temperature. The time interval between consecutive pBoc contractions was scored for 11 consecutive pBoc contractions. For each strain, 6-10 worms were analyzed. Statistical analysis was performed using ANOVA followed by Tukey's multiple comparison tests using Prism 5.0 (GraphPad software).

Supplemental Data

Four figures, two movies, two tables, and Supplemental Experimental Procedures are available as Supplemental Data.

Acknowledgments

Some strains used in this study were obtained from the *C. elegans* Genetics Center (CGC), which is supported by a grant from the National Institutes of Health (NIH, National Center for Research Resources). This work was supported by NIH grant R15-GM084451 to A.L.A, NSF grant IOS0919848 to K.W.N. and an NSF-RUI 0842830 grant to M.A.P.

Reference

1. Baruscotti M., Barbuti A., and Bucchi A. (2010). The cardiac pacemaker current. J. Mol. Cell. Cardiol. 48, 55-64.
2. Berridge M.J. (2008). Smooth muscle cell calcium activation mechanisms. The J. Physiol. 586, 5047-5061.
3. Irisawa H., Brown H.F., and Giles W. (1993). Cardiac pacemaking in the sinoatrial node. Physiol. Rev. 73, 197-227.
4. Sanders K.M., Koh S.D., and Ward S.M. (2006). Interstitial cells of cajal as pacemakers in the gastrointestinal tract. Ann. Rev. Physiol. 68, 307-343.
5. Avery L., and Thomas J.H. (1997). Feeding and Defecation. In *C. elegans* II, D.L. Riddle, T. Blumenthal, B.J. Meyer, and J.R. Priess, eds. (Cold Spring Harbor, NY: Cold Spring Harbor Laboratory Press), pp. 679–716.
6. McCarter J., Bartlett B., Dang T., and Schedl T. (1999). On the control of oocyte meiotic maturation and ovulation in *Caenorhabditis elegans*. Dev. Biol. 205, 111-

128.
7. Thomas J.H. (1990). Genetic analysis of defecation in *Caenorhabditis elegans*. Genetics 124, 855-872.
8. Allman E., Thyagarajan B., and Nehrke K. (2012). The inositol 1, 4, 5-trisphosphate receptor in *C. elegans*. WIREs Membr. Transp. Signal 1, 321-328.
9. Dal Santo P., Logan M.A., Chisholm A.D., and Jorgensen E.M. (1999). The inositol trisphosphate receptor regulates a 50-second behavioral rhythm in *C. elegans*. Cell 98, 757-767.
10. Espelt M.V., Estevez A.Y., Yin X., and Strange K. (2005). Oscillatory Ca^{2+} signaling in the isolated *Caenorhabditis elegans* intestine: role of the inositol-1,4,5-trisphosphate receptor and phospholipases C beta and gamma. J. Gen. Physiol. 126, 379-392.
11. Teramoto T., and Iwasaki K. (2006). Intestinal calcium waves coordinate a behavioral motor program in *C. elegans*. Cell Calcium 40, 319-327.
12. Kwan C.S., Vázquez-Manrique R.P., Ly S., Goyal K., and Baylis H.A. (2008). TRPM channels are required for rhythmicity in the ultradian defecation rhythm of *C. elegans*. BMC Physiol. 8, 11.
13. Xing J., Yan X., Estevez A., and Strange K. (2008). Highly Ca2+-selective TRPM channels regulate IP_3-dependent oscillatory Ca2+ signaling in the *C. elegans* intestine. J. Gen. Physiol. 131, 245-255.
14. Xing J., and Strange K. (2010). Phosphatidylinositol 4,5-bisphosphate and loss of PLCgamma activity inhibit TRPM channels required for oscillatory Ca2+ signaling. Am J Physiol, Cell Physiol. 298, C274-82.
15. Beg A.A., Ernstrom G.G., Nix P., Davis M.W., and Jorgensen E.M. (2008). Protons act as a transmitter for muscle contraction in *C. elegans*. Cell 132, 149-160.
16. Pfeiffer J., Johnson D., and Nehrke K. (2008). Oscillatory transepithelial H(+) flux regulates a rhythmic behavior in *C. elegans*. Curr. Biol. 18, 297-302.
17. McGhee J.D. (2007). The *C. elegans* intestine. WormBook : the online review of C elegans biology 1-36.
18. Peters M.A., Teramoto T., White J.Q., Iwasaki K., and Jorgensen E.M. (2007). A calcium wave mediated by gap junctions coordinates a rhythmic behavior in *C. elegans*. Curr. Biol. 17, 1601-1608.
19. Nehrke K., Denton J., and Mowrey W. (2008). Intestinal Ca2+ wave dynamics in freely moving *C. elegans* coordinate execution of a rhythmic motor program. AJP - Cell Physiol. 294, C333.
20. Bartel D.P. (2009). MicroRNAs: target recognition and regulatory functions. Cell 136, 215-233.
21. Stefani G., and Slack F. (2008). Small non-coding RNAs in animal development. Nat. Rev. Mol. Cell. Biol. 9, 219-230.
22. Miska E.A., Alvarez-Saavedra E., Abbott A.L., Lau N.C., Hellman A.B., McGonagle S.M., Bartel D.P., Ambros V.R., and Horvitz H.R. (2007). Most *Caenorhabditis elegans* microRNAs are individually not essential for development or viability. PLoS Genet. 3, e215.
23. Kniazeva M., Sieber M., Mccauley S., Zhang K., Watts J.L., and Han M. (2003). Suppression of the ELO-2 FA elongation activity results in alterations of the fatty acid composition and multiple physiological defects, including abnormal ultradian

rhythms, in *Caenorhabditis elegans*. Genetics 163, 159-169.
24. Martinez N.J., Ow M.C., Reece-Hoyes J.S., Barrasa M.I., Ambros V.R., and Walhout A.J. (2008). Genome-scale spatiotemporal analysis of *Caenorhabditis elegans* microRNA promoter activity. Genome Res. 18, 2005-2015.
25. Branicky R., and Hekimi S. (2006). What keeps *C. elegans* regular: the genetics of defecation. Trends Genet. 22, 571-579.
26. Walker D.S., Gower N.J.D., Ly S., Bradley G.L., and Baylis H.A. (2002). Regulated disruption of inositol 1,4,5-trisphosphate signaling in *Caenorhabditis elegans* reveals new functions in feeding and embryogenesis. Mol. Biol. Cell 13, 1329-1337.
27. Palmer A.E., Giacomello M., Kortemme T., Hires S.A., Lev-Ram V., Baker D., and Tsien R.Y. (2006). Ca^{2+} indicators based on computationally redesigned calmodulin-peptide pairs. Chem Biol 13, 521-530.
28. Hammell M., Long D., Zhang L., Lee A., Carmack C.S., Han M., Ding Y., and Ambros V. (2008). mirWIP: microRNA target prediction based on microRNA-containing ribonucleoprotein-enriched transcripts. Nature Methods 5, 813-819.
29. Kertesz M., Iovino N., Unnerstall U., Gaul U., and Segal E. (2007). The role of site accessibility in microRNA target recognition. Nat. Genet. 39, 1278-1284.
30. Jan C.H., Friedman R.C., Ruby J.G., and Bartel D.P. (2011). Formation, regulation and evolution of *Caenorhabditis elegans* 3'UTRs. Nature 469, 97-101.
31. Lewis B.P., Burge C.B., and Bartel D.P. (2005). Conserved seed pairing, often flanked by adenosines, indicates that thousands of human genes are microRNA targets. Cell 120, 15-20.
32. Lackner M.R., Nurrish S.J., and Kaplan J.M. (1999). Facilitation of synaptic transmission by EGL-30 Gqalpha and EGL-8 PLCbeta: DAG binding to UNC-13 is required to stimulate acetylcholine release. Neuron 24, 335-346.
33. Miller K.G., Emerson M.D., and Rand J.B. (1999). Goalpha and diacylglycerol kinase negatively regulate the Gqalpha pathway in *C. elegans*. Neuron 24, 323-333.
34. Mukherji S., Ebert M.S., Zheng G.X.Y., Tsang J.S., Sharp P.A., and van Oudenaarden A. (2011). MicroRNAs can generate thresholds in target gene expression. Nat. Genet. 43, 854-859.
35. Shipston M.J. (2011). Ion channel regulation by protein palmitoylation. J. Biol. Chem. 286, 8709-8716.
36. Smotrys J.E., and Linder M.E. (2004). Palmitoylation of intracellular signaling proteins: regulation and function. Annu. Rev. Biochem. 73, 559-587.
37. Ren J., Wen L., Gao X., Jin C., Xue Y., and Yao X. (2008). CSS-Palm 2.0: an updated software for palmitoylation sites prediction. Protein Eng. Des. Sel. 21, 639-644.

Figure Legends

Figure 1. *mir-240/786* is expressed in intestinal cells.
(A) Alignment of miR-193b and miR-365a in humans with miR-240 and miR-786 in *C. elegans*, respectively. Dots indicate bases conserved between humans and *C. elegans*. (B) The *mir-240* and *mir-786* sequences are separated by only 100 nt on the X chromosome. The deletion, *n4541*, removes 1185 bp. Rescuing activity was observed with a genomic

fragment that contains *mir-786*. (C) Schematic of *C. elegans* intestine with a series of 9 rings of cells from the anterior int1 to the posterior int9. Modified from [17]. (D,E) Representative confocal images of the *mir-240/786* promoter driving GFP expression (*mir-240/786*^{prom}*::gfp)*. Anterior is to the left. Scale bar = 20 μm. (D) Weak GFP expression is observed in the int1 anterior ring of cells. No expression is observed in the pharynx in adult worms. (E) GFP expression is observed in the posterior int9 cells. Expression is also observed in the gonadal sheath cells.

Figure 2. Loss of *mir-240/786* results in long arrhythmic defecation cycles.
(A) Diagram of the three contractions of the DMP in *C. elegans*. A posterior body contraction (pBoc) pushes the contents of the intestine towards the anterior. An anterior contraction (aBoc) just behind the pharynx occurs about 3-4 s later that pushes intestinal contents towards the posterior. An enteric muscle contraction (EMC) follows ~1 s later resulting in an expulsion. In wild-type worms, the DMP is executed every ~50 s (B-C) Analysis of defecation cycle times (s) in individual worms. Individual cycle times for each worm are denoted by dots. 10 defecation cycles were analyzed in 10 individual and the mean is listed as a solid line for (B) wild-type worms and (C) *mir-240/786* mutant worms.

Figure 3. Elevation of IP_3 receptor activity can suppress *mir-240/786* defecation defects. (A) IP_3-mediated pathway for calcium release. Hydrolysis of PIP_2 generates IP_3, which can be converted to IP_4 by the IP_3 kinase, LFE-2, or to IP_2 by the IP_3 phosphatase, IPP-5. IP_3 binds to its receptor, ITR-1, on the endoplasmic reticulum (ER), resulting in the release of intracellular calcium. (B) Average defecation cycle times (mean + SD) for wild-type and mutant worms. The average defecation cycle time as determined by the time between consecutive posterior body contractions (n = 5-10 worms, 10 cycles/worm). Genetic analysis was performed in the *unc-24(e138)* genetic background because available gain-of-function alleles of *itr-1* are linked to this allele, For *lfe-2,* genetic analysis was performed in the *unc-38(x20)* genetic background because the available *lfe-2(sy326)* allele is linked to *unc-38(x20)*. (C) Variation of cycle time (mean + SD) for wild-type and mutant worms. The average coefficient of variation was calculated for 5-10 worms for each strain. * $p < 0.01$ one way ANOVA and Tukey's test. ns, not significant, $p > 0.05$.

Figure 4. *mir-240/786* spatially constrains calcium wave initiation.
Calcium was measured using dynamic imaging of live transgenic *C. elegans* expressing the dual emission fluorescent FRET-based calcium sensor D3cpV in the intestine, while pH was measured using fluorescent imaging of worms expressing the dual excitation pH biosensor pHluorin. (A) A representative trace of oscillations in average intestinal calcium (R/R_0) in a congenic wild-type control worm. (B) Representative intestinal pH oscillations in a congenic wild-type control worm. (C) Three intestinal calcium traces from *mir-240/786* mutant worms, with the y-axis scaled to wild-type and the individual traces offset from each other for clarity. (D) Representative pH oscillations in *mir-240/786* mutants, as above. For the graphs shown in A-D, the execution of the DMP is noted by block arrows color-coded to the corresponding traces, located above the graph. (E) An intestinal calcium heat map (red = elevated) illustrates ectopic calcium signals in

mir-240/786 mutants. In this representative case, a calcium signal arising in the cells proximal to the posterior intestine propagates in reverse and triggers a minor contraction of the posterior body wall muscles (small arrow). This is followed shortly thereafter by a more robust increase in calcium, a second contraction, a calcium wave propagating in the forward direction, and execution of the full DMP (large arrow). (F) A representative intestinal pH heat map (blue = acidic) where a weak pBoc (small arrow) is shown occurring in the absence of overt acidification, followed shortly thereafter by robust acidification and full DMP (large arrow). (G) The supremacy of the posterior cell as pacemaker was quantified in control and mutant worms by assessing the initial site of calcium signaling that ultimately resulted in execution of the DMP. Calcium waves that initiated in the posterior and anterior cells nearly simultaneously were classified as normal. Signals arising elsewhere or in the anterior intestine alone were classified as aberrant (H) The number of calcium signaling events ($\sim R/R_0 > 1.1$) per expulsion step was determined using fluorescent imaging (for both G and H, 300s imaging per worm, n=8 for wild-type controls; n=10 for *mir-240/786* mutants).

Figure 5. *elo-2* is likely a direct target of miR-786.
(A) Knockdown of *elo-2* results in shorter defecation cycles in wild-type and *mir-240/786* worms. *, $p < 0.05$, ** $p < 0.01$ one way ANOVA and Tukey's test. ns, not statistically significant, $p > 0.05$. (B) Sequence of a putative miR-786 binding site within the *elo-2* 3'UTR. The miR-786 alignment with the *elo-2* 3' UTR is adapted from the mirWIP database [28]. (C) Representative traces of intestinal calcium oscillations in a *mir-240/786;elo-2(RNAi)* mutant worm (black) and a control *elo-2(RNAi)* worm (dashed). The traces have been offset from each other for clarity. The execution of the defecation motor program is noted by block arrows color-coded to the corresponding traces. (D) The supremacy of the posterior cell as pacemaker was quantified by assessing the initial site of calcium signaling that ultimately resulted in execution of the defecation motor program. Calcium waves that initiated in the posterior and anterior cells nearly simultaneously were classified as normal. Signals arising elsewhere or in the anterior intestine alone were classified as ectopic. (E) Representative fluorescent micrograph with (F) corresponding DIC image of the posterior intestine of a wild-type worm expressing low $elo\text{-}2^{prom}::gfp::elo\text{-}2^{3'\,UTR}$ transgene expression in int9 posterior intestinal cells. (G) Worms were categorized based on the relative GFP expression level between int9 and their neighboring int8 cells. The percentage of worms that displayed low GFP expression in int9 relative to int8 was compared in wild-type and *mir-240/786* mutants. Expression was observed from a transgene under the regulation of the *elo-2* 3' UTR as well as the *elo-2* 3' UTR in which the predicted miR-786 binding site was deleted (3' UTRmut). * $p < 0.01$ by Chi-square analysis. ns, not significant. (H) Palmitate supplementation suppresses the long defecation cycle defects of *mir-240/786* mutants. *, $p < 0.01$ Two-way ANOVA and Bonferroni's test. (I) Model for miR-786 function. Our data suggests that miR-786 repression of *elo-2* may regulate protein palmitoylation or membrane lipid composition to control calcium signaling in the intestine.

Figure 1

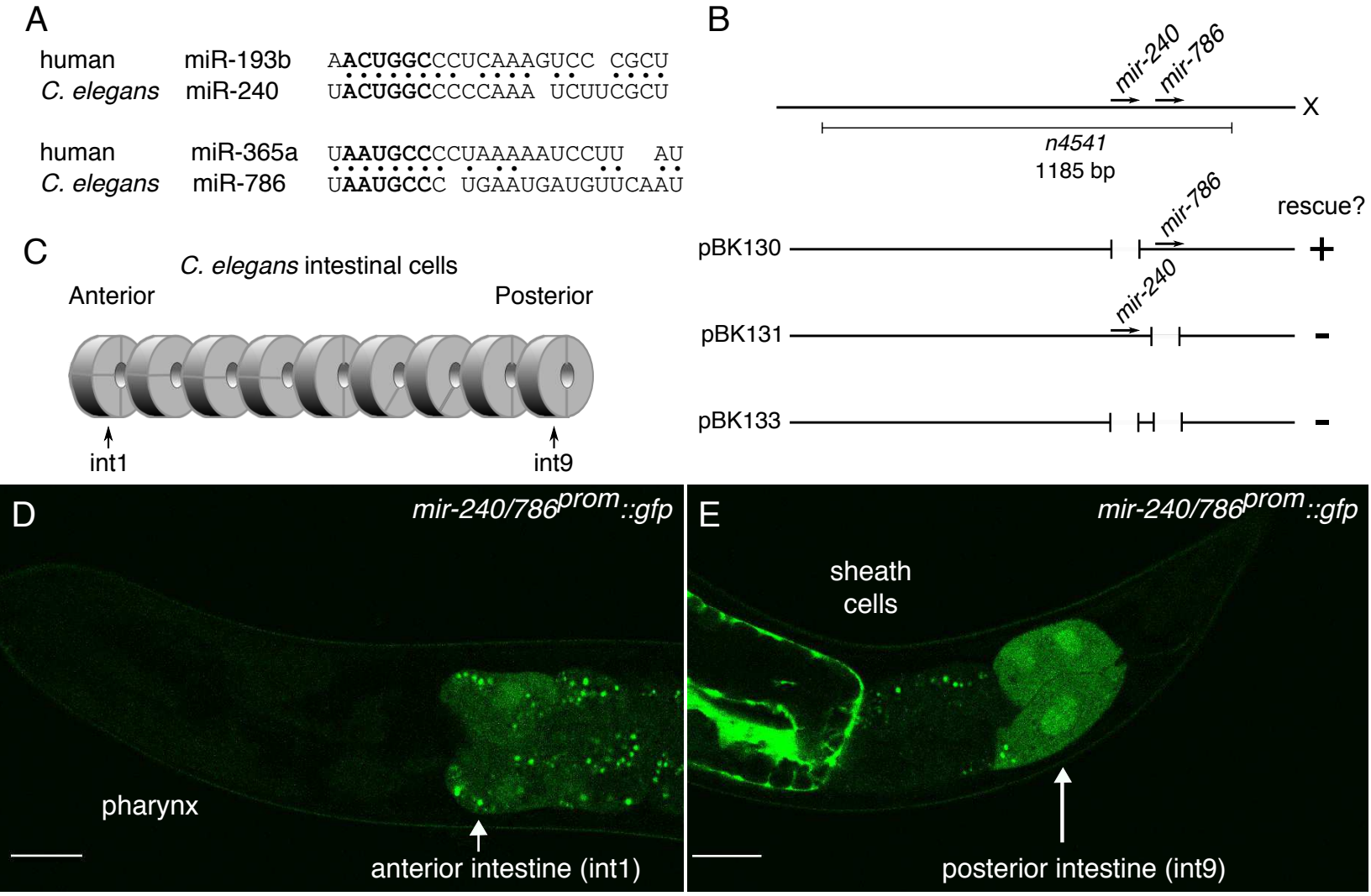
A
human miR-193b AACUGGCCCUCAAAGUCC CGCU
C. elegans miR-240 UACUGGCCCCCAAA UCUUCGCU
human miR-365a UAAUGCCCCUAAAAAUCCUU AU
C. elegans miR-786 UAAUGCCC UGAAUGAUGUUCAAU
B
mir-240
mir-786
X
n4541
1185 bp
rescue?
pBK130
pBK131
pBK133
C
C. elegans intestinal cells
Anterior
Posterior
int1
int9
D
mir-240/786prom::gfp
pharynx
anterior intestine (int1)
E
mir-240/786prom::gfp
sheath cells
posterior intestine (int9)

Figure 2

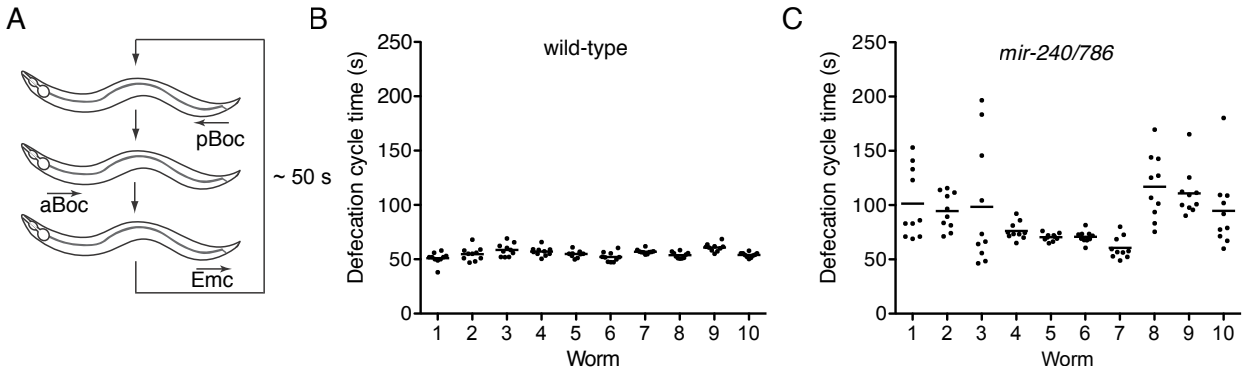
A
pBoc
aBoc
Emc
~ 50 s
B
wild-type
Defecation cycle time (s)
250
200
150
100
50
0
1 2 3 4 5 6 7 8 9 10
Worm
C
mir-240/786
Defecation cycle time (s)
250
200
150
100
50
0
1 2 3 4 5 6 7 8 9 10
Worm

Figure 3

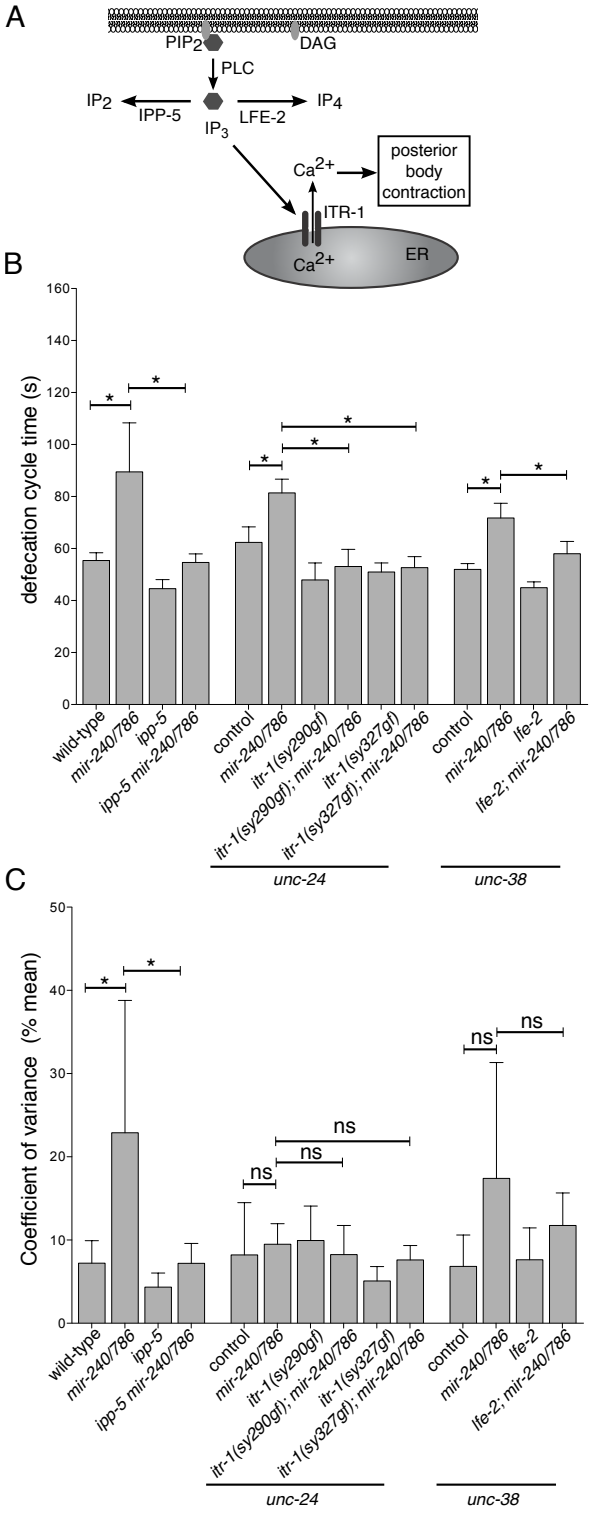
A
PIP2
DAG
PLC
IP2
IPP-5
IP3
LFE-2
IP4
Ca2+
posterior body contraction
ITR-1
Ca2+
ER
B
defecation cycle time (s)
wild-type
mir-240/786
ipp-5
ipp-5 mir-240/786
control
mir-240/786
itr-1(sy290gf)
itr-1(sy290gf); mir-240/786
itr-1(sy327gf)
itr-1(sy327gf); mir-240/786
control
mir-240/786
lfe-2
lfe-2; mir-240/786
unc-24
unc-38
C
Coefficient of variance (% mean)
ns

Figure 4

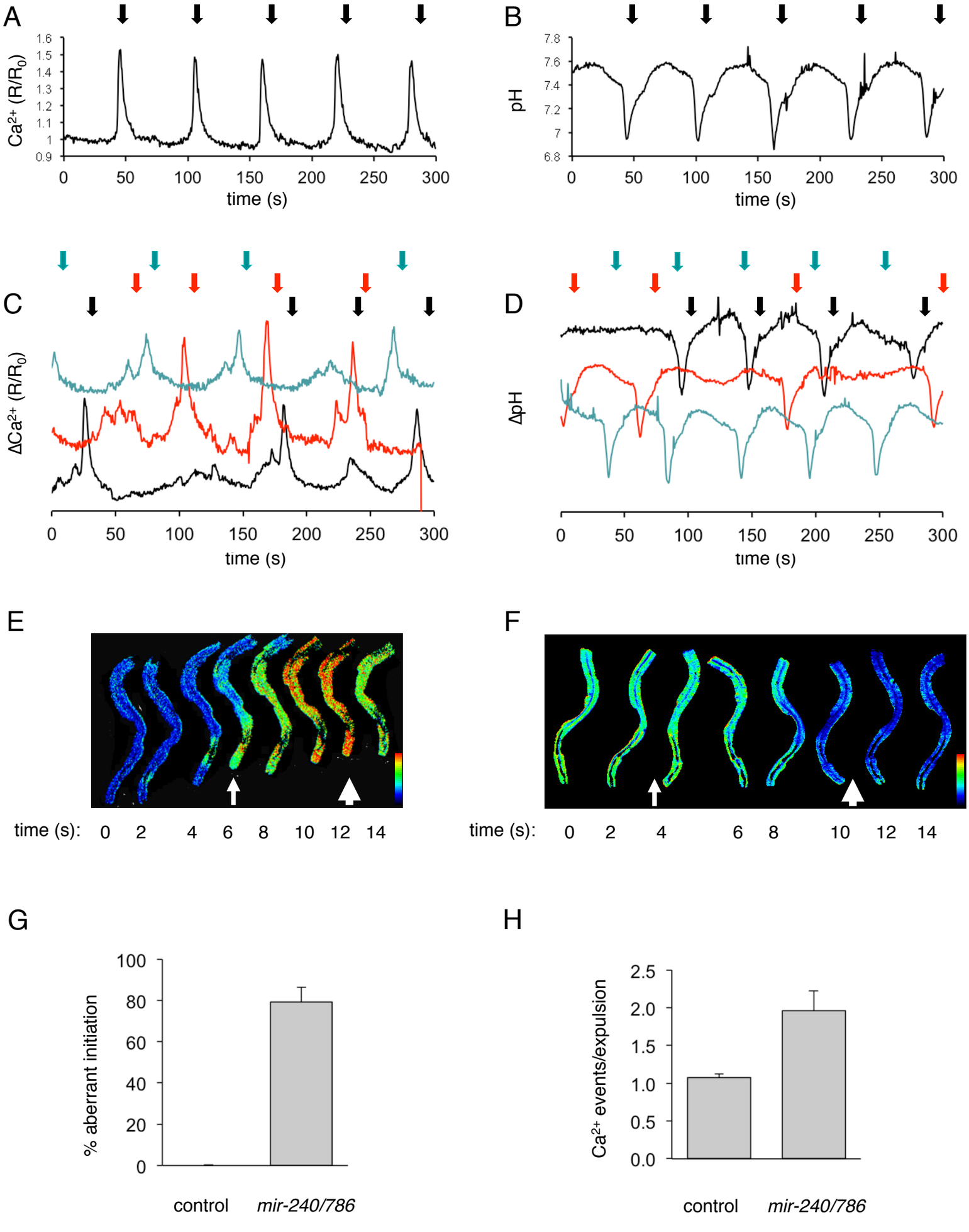
A
Ca2+ (R/R0)
time (s)
B
pH
time (s)
C
ΔCa2+ (R/R0)
time (s)
D
ΔpH
time (s)
E
time (s): 0 2 4 6 8 10 12 14
F
time (s): 0 2 4 6 8 10 12 14
G
% aberrant initiation
control
mir-240/786
H
Ca2+ events/expulsion
control
mir-240/786

Figure 5

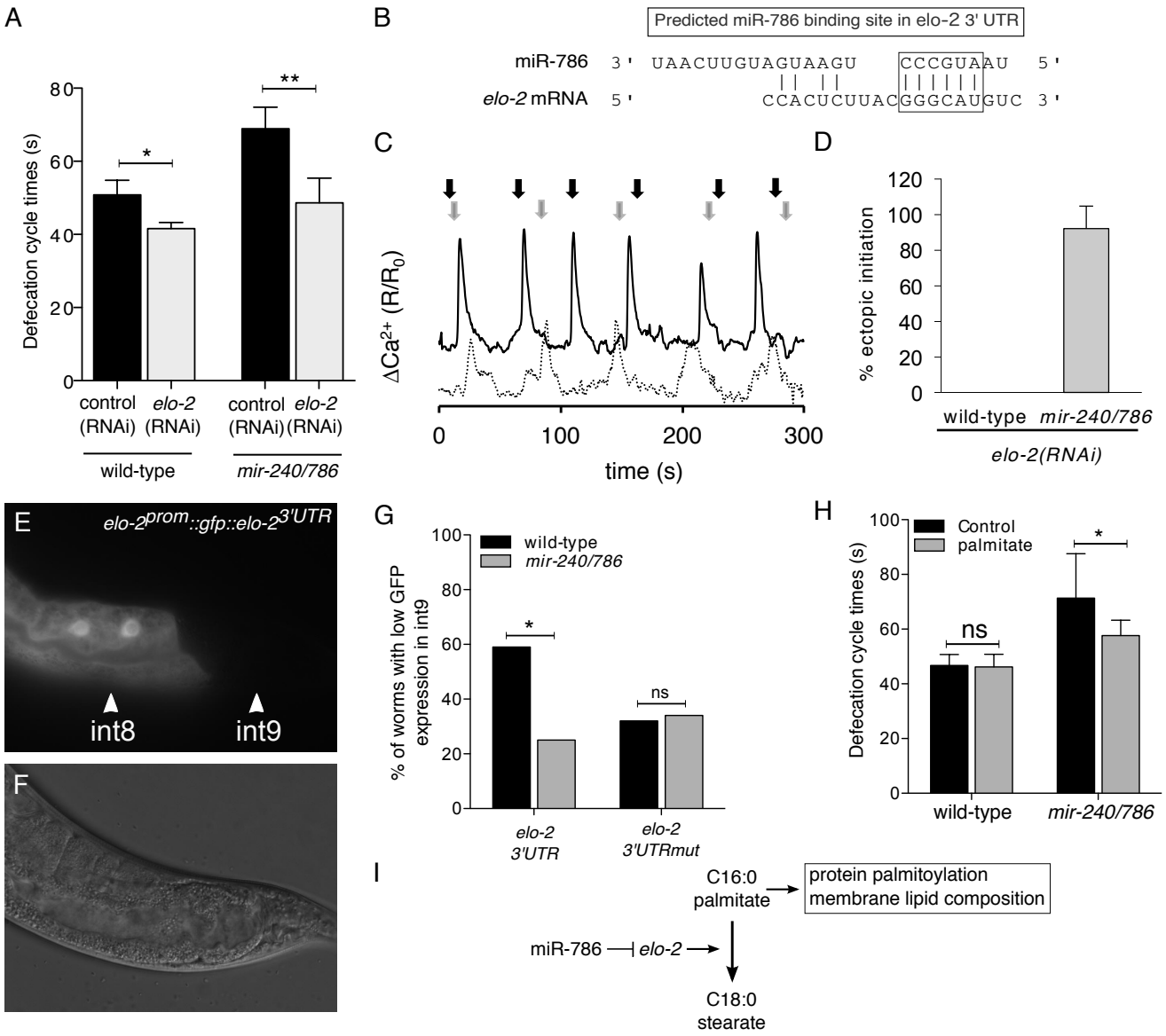
A
Defecation cycle times (s)
control (RNAi)
elo-2 (RNAi)
wild-type
mir-240/786
B
Predicted miR-786 binding site in elo-2 3' UTR
miR-786 3' UAACUUGUAGUAAGU CCCGUAAU 5'
elo-2 mRNA 5' CCACUCUUACGGGCAUGUC 3'
C
ΔCa2+ (R/R0)
time (s)
D
% ectopic initiation
wild-type
mir-240/786
elo-2(RNAi)
E
elo-2prom::gfp::elo-23'UTR
int8
int9
F
G
% of worms with low GFP expression in int9
wild-type
mir-240/786
elo-2 3'UTR
elo-2 3'UTRmut
ns
H
Defecation cycle times (s)
Control
palmitate
ns
wild-type
mir-240/786
I
C16:0 palmitate
protein palmitoylation
membrane lipid composition
miR-786
elo-2
C18:0 stearate

Inventory of Supplemental Information

1. Supplemental Figures, Movies, and Tables
    Figure S1, related to Figure 4
    Figure S2, related to Figure 3
    Figure S3, related to Figure 5
    Movie S1, related to Figure 2
    Movie S2, related to Figure 4
    Table S1, related to Figure 1 and 5
    Table S2, related to Figure 5
    Table S3, related to Experimental procedures

2. Supplemental Experimental Procedures

3. Supplemental References

Figure S1

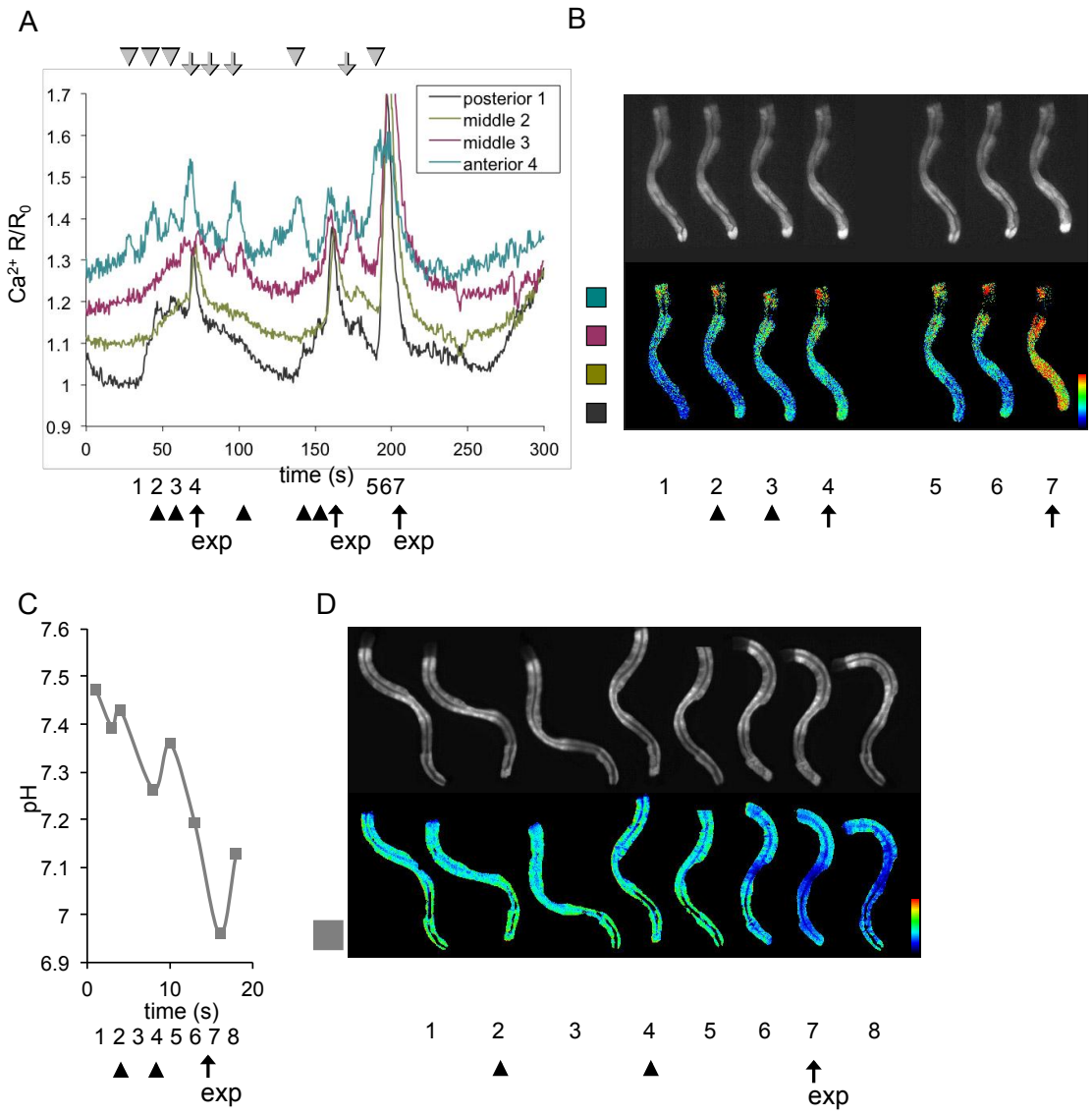

Figure S1. *mir-240/786* is an amplifier of calcium signaling in the posterior-most cells of the *C. elegans* intestine. (A) Calcium traces were obtained from four regions-of-interest throughout the intestine in a *mir-240/786* mutant worm, with the regions-of-interest depicted by the colored boxes in panel B and the corresponding data plotted as a line of the same color. These data

indicate that small oscillations in calcium occur independently in the anterior (gray arrows) and posterior (black arrows) cells of the intestine. Though *mir-240/786* mutant worms can exhibit calcium signals that initiate in internal cells, as shown in Figure 4, this particular mutant worm does not. Oscillations that are cell-restricted are depicted by arrowheads and oscillations that initiate wave propagation are shown by arrows. The directionality of the wave is determined by its site of initiation, with reverse waves traveling much slower than forward waves. While reverse waves may cause a contraction (see Figure 4 and t = ~100 seconds here) they are generally incapable of triggering the defecation motor program. However, forward waves are often preceded by "false starts" or minor signaling events that are restricted to the posterior-most cells. (B) Single wavelength and calcium heat maps extracted at times 1-7, as annotated in panel A, are representative of both behavioral and signaling events commonly observed in *mir-240/786* mutants. The images from times 1-3 illustrate how cell-restricted elevations in calcium can occur prior to forward wave initiation (time 4) and are associated with small contractions of the posterior intestine, as can be seen clearly in the single wavelength images. The weak calcium wave shown at time 4 never reaches the anterior intestinal cell, which continues to oscillate independently, consistent with the idea that calcium is its own timer and can reset the oscillatory clock. Times 5-7 are more akin to what is generally observed in wild-type worms, and consistent with a calcium reset, this robust signaling event is sufficient to inhibit subsequent minor calcium oscillations throughout the intestine. Overall, these data support the idea that *mir-240/786* amplifies calcium signaling and that robust signaling drives wave propagation from the posterior intestinal cell, inhibiting calcium oscillations in other cells and establishing its supremacy as the defecation pacemaker. (C-D) Rhythmic acidification of the posterior-most intestinal cells coincides with the minor contractions observed preceding the defecation motor program. (C) The pH of the posterior-most intestinal cells, as indicated by the grey box in panel B, was determined prior to and during execution of the defecation motor program. Minor contractions are depicted by arrowheads and the defecation motor program is depicted by an arrow. (D) Single wavelength and pH heat maps were extracted at times 1-8, as indicated, and clearly demonstrate that a slight acidification occurs with each minor contraction (arrowheads) that precedes the DMP (arrow). The extent of the acidification and contraction appear to increase rhythmically, reminiscent of the sequential increases in calcium that precede the defecation motor program.

Figure S2

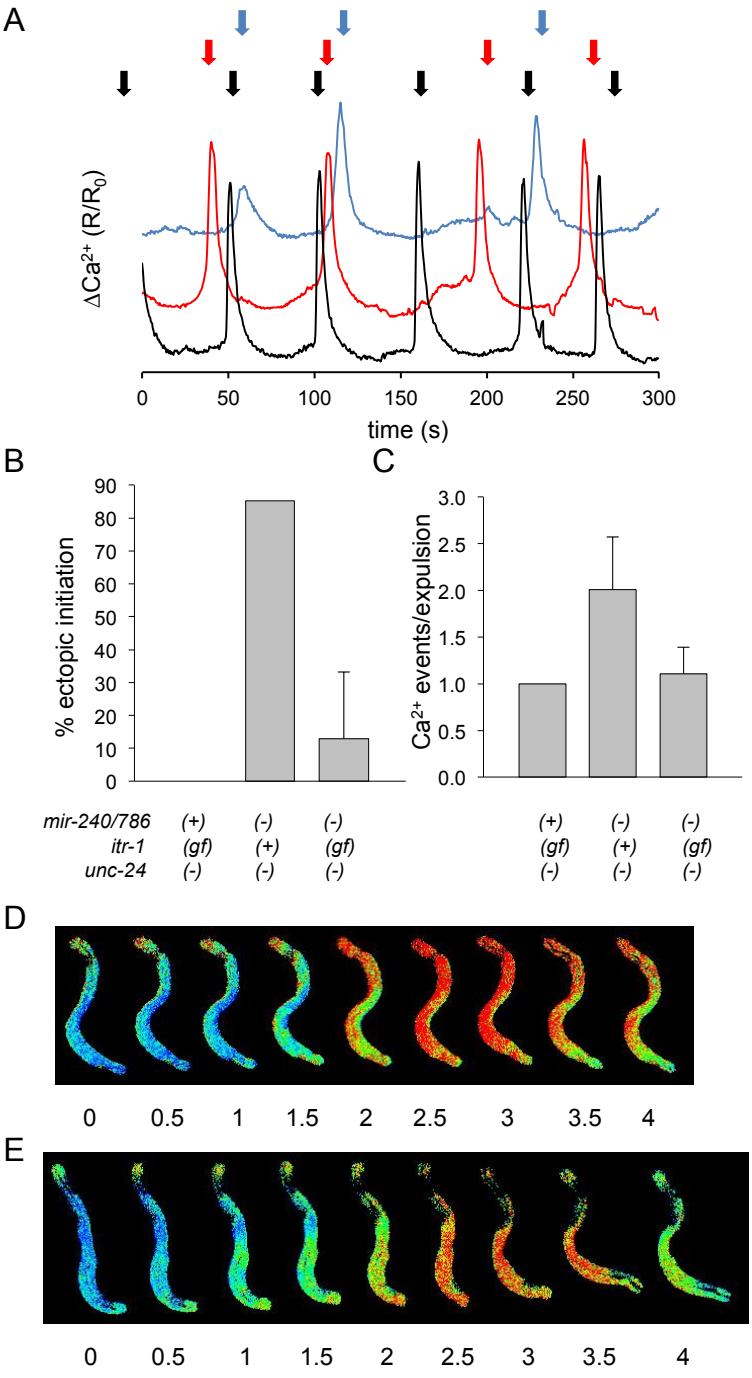
A
ΔCa2+ (R/R0)
0
50
100
150
200
250
300
time (s)
B
% ectopic initiation
90
80
70
60
50
40
30
20
10
0
C
Ca2+ events/expulsion
3.0
2.5
2.0
1.5
1.0
0.5
0.0
mir-240/786 (+) (-) (-)
itr-1 (gf) (+) (gf)
unc-24 (-) (-) (-)
(+) (-) (-)
(gf) (+) (gf)
(-) (-) (-)
D
0 0.5 1 1.5 2 2.5 3 3.5 4
E
0 0.5 1 1.5 2 2.5 3 3.5 4

Figure S2 *itr-1(gf)* suppresses ectopic calcium wave initiation. (A) Representative traces of intestinal calcium oscillations in *mir-240/786* (blue), *itr-1(sy327gf)* (black), *itr-1(sy327gf); mir-240/786* (red). Analysis was performed in the *unc-24(e138)* genetic background as discussed in the text. The traces have been offset for clarity. The execution of the defecation motor program is noted by block arrows color-coded to the corresponding traces, located above the graph. (B) The supremacy of the posterior cell as pacemaker was quantified by assessing the initial site of calcium signaling that ultimately resulted in execution of the defecation motor program. Calcium waves that initiated in the posterior and anterior cells nearly simultaneously were classified as normal. Signals arising elsewhere or in the anterior intestine alone were classified as aberrant. (C) The number of calcium signaling events ($\sim R/R_0 > 1.1$) per expulsion step was determined. (C-D) The data was analyzed from 300 s of imaging per worm, n=3 worms for *itr-1(sy327gf); mir-240/786*, n=7 worms for *itr-1(sy327gf)*, n=7 worms for *mir-240/786* (C, D) Calcium heat maps (red=elevated) were derived from data extracted at the time points indicated (in seconds) from dynamic fluorescent imaging experiments to illustrate how *itr-1(gf)* influences the spatial dynamics of calcium signals in (D) *itr-1(sy327gf)* and (E) *itr-1(sy327gf)*; *mir-240/786* worms.

Figure S3

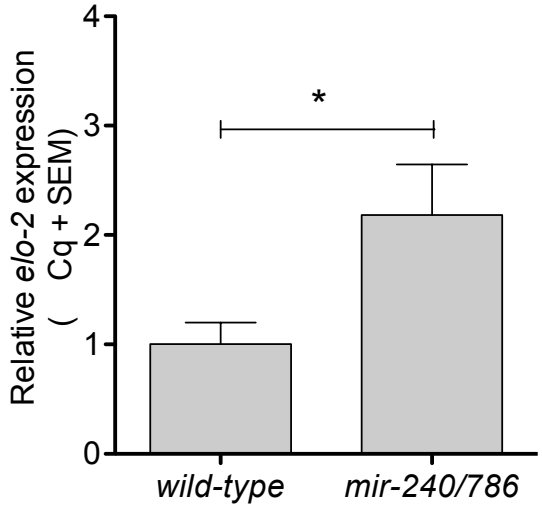

Figure S3. *mir-240/786* mutants display a modest increase in *elo-2* mRNA levels compared to wild-type worms at the young adult stage. Real time qPCR was performed with two biological replicate RNA preparations, the average ΔΔCq + SEM is shown (Bio-Rad CFX Manager software). Data from two technical replicates of the experiment were analyzed with 2-way ANOVA, significance of difference between wild-type and *mir-240/786*, p = 0.0372.

Movie S1. Defecation Motor Program in wild-type and *mir-240/786* worms. This movie includes representative sequences showing a wild-type defecation motor program, *mir-240/786* biphasic posterior body contraction, expulsion failure, and a weak posterior body contraction, as indicated by title panels. Related to Figure 2.

Movie S2. Calcium oscillations in wild-type and *mir-240/786* worms. This movie includes representative sequences showing calcium oscillations in wild-type and *mir-240/786* worms, as indicated by title panels. Related to Figure 4E.

Table S1: Rescue data for defecation defects in *mir-240/786(n4541)* mutant worms.

Strain	Genotype	*mir-240*	*mir-786*	Average defecation cycle time (s)	% CV[a]	n[b]	Rescue
RF117	*mir-240/786 (n4541) X; nEx1459*	+	+	59.0	8.6	6	yes
RF579	*mir-240/786 (n4541) X; xwEx82*	-	+	61.3	9.9	6	yes[c]
RF580	*mir-240/786 (n4541) X; xwEx83*	-	+	61.9	6.7	6	yes[c]
RF581	*mir-240/786 (n4541) X; xwEx84*	-	+	57.4	13.3	6	yes[c]
RF593	*mir-240/786 (n4541) X; xwEx85*	+	-	70.4	18.3	6	no[d]
RF595	*mir-240/786 (n4541) X; xwEx86*	+	-	73.7	30.8	10	no[d]
RF596	*mir-240/786 (n4541) X; xwEx87*	+	-	70.4	25.1	11	no[d]
RF633	*mir-240/786 (n4541) X; xwEx91*	-	-	73.2	20.7	6	no[d]
RF634	*mir-240/786 (n4541) X; xwEx92*	-	-	69.5	20.5	6	no[d]
RF635	*mir-240/786 (n4541) X; xwEx93*	-	-	70.0	25.1	6	no[d]

[a] % CV, coefficient of variance
[b] number of worms
[c] indicates rescuing activity statistically equivalent compared to RF117, $p > 0.05$
[d] indicates rescuing activity statistically different compared to RF117, $p < 0.05$

Table S2: RNAi analysis of computationally-predicted miR-786 targets

	wild-type				*mir-240/786*			
RNAi	Average Defecation time (s)	SD	%CV[a]	n	Average Defecation time (s)	SD	%CV	n
empty	50.9	3.9	7.8	5	66.63	5.9	8.9	6
elo-2	41.6	1.7	4.1	6	48.67[b]	6.7	13.8	6
unc-70	60.9	4.6	7.6	6	69.12	7.9	11.5	6
Y65B4BL.5	48.4	2.0	4.2	6	73.17	8.3	11.3	5
mig-15	50.6	1.7	3.3	6	75.67	10.3	13.6	6
F36A2.9	50.7	2.3	4.5	6	69.31	8.6	12.5	6
F52E1.13	59.5	4.0	6.7	6	71.77	3.6	5.0	6
unc-22	61.2	7.7	12.5	6	66.75	13.7	20.6	6
ncx-2	53.0	5.5	10.4	6	62.92	5.5	8.8	5
rab-10	106.4[c]	26.2	24.6	6	92.19[b]	18.0	19.6	6
tkt-1	47.8	0.7	1.5	6	67.10	2.8	4.2	6
T04B2.5	52.2	2.5	4.8	6	75.20	5.2	6.9	6
T26A5.6	49.5	2.9	5.9	6	76.80	4.8	6.3	6
crh-2	53.9	5.9	11.0	6	68.98	3.7	5.4	6
ceh-38	46.1	7.7	16.6	6	61.37	8.6	13.9	6
sms-3	53.3	2.6	4.9	6	69.28	8.5	12.2	6
ifc-2	48.5	4.8	10.0	6	68.08	16.0	23.5	6
igcm-3	57.3	7.3	12.7	6	79.78	18.4	23.0	6
lst-1	51.4	2.9	5.7	6	87.72[b]	11.9	13.6	6
frl-1	48.5	2.8	5.8	6	65.98	12.0	18.2	6
mca-3	48.5	2.4	4.9	6	74.30	9.0	12.2	6
kcc-1	55.6	2.3	4.1	6	76.27	6.8	8.9	6
rlbp-1	51.1	5.3	10.4	6	65.58	8.4	12.8	6
fli-1	52.8	3.8	7.2	6	79.27	19.1	24.1	6

[a] % CV, coefficient of variation
[b] different from *mir-240/786 (*empty*),* $p < 0.01$
[c] different from wild-type (empty), $p < 0.01$

Table S3. List of Genetic Strains

Strain name	description	Full genotype
N2	wild-type	
RF61	*mir-240/786*	*mir-240/786(n4541) X.*
RF656	*mir-240/786^{prom}::GFP*	*unc-119(ed3) III; wwIs5 [unc-119(+) + mir-240/786^{prom}::GFP].* 2x backcrossed
RF117	rescue	*mir-240/786(n4541) X; nEx1459 [sur-5::gfp + mir-240(+) mir-786(+)]*
RF579	rescue	*mir-240/786 (n4541) X; xwEx82 [sur-5::gfp + mir-240(-) mir-786(+)].*
RF580	rescue	*mir-240/786 (n4541) X; xwEx83 [sur-5::gfp + mir-240(-) mir-786(+)].*
RF581	rescue	*mir-240/786 (n4541) X; xwEx84 [sur-5::gfp + mir-240(-) mir-786(+)].*
RF593	rescue	*mir-240/786 (n4541) X; xwEx85 [sur-5::gfp + mir-240(+) mir-786(-)].*
RF595	rescue	*mir-240/786 (n4541) X; xwEx86 [sur-5::gfp + mir-240(+) mir-786(-)].*
RF596	rescue	*mir-240/786 (n4541) X; xwEx87 [sur-5::gfp + mir-240(+) mir-786(-)].*
RF633	rescue	*mir-240/786 (n4541) X; xwEx91 [sur-5::gfp + mir-240(-) mir-786(-)].*
RF634	rescue	*mir-240/786 (n4541) X; xwEx92 [sur-5::gfp + mir-240(-) mir-786(-)].*
RF635	rescue	*mir-240/786 (n4541) X; xwEx93 [sur-5::gfp + mir-240(-) mir-786(-)].*
PS3653	*ipp-5*	*ipp-5(sy605) X.*
RF571	*ipp-5 mir-240/786*	*ipp-5(sy605) mir-240/786(n4541) X.*
CB138	*unc-24*	*unc-24(e138) IV.*
RF567	*unc-24; mir-240/786*	*unc-24(e138) IV; mir-240/786(n4541) X.*
PS2582	*unc-24 itr-1(sy290gf)*	*itr-1(sy290) unc-24(e138) IV.*
RF523	*unc-24 itr-1 (sy290gf); mir-240/786*	*itr-1(sy290) unc-24(e138) IV; mir-240/786(n4541) X.*
PS2368	*unc-24 itr-1(sy327gf)*	*itr-1(sy327) unc-24(e138) IV*
RF520	*unc-24 itr-1(sy327gf); mir-240/786*	*itr-1(sy327) unc-24(e138) IV; mir-240/786(n4541) X.*
ZZ20	*unc-38*	*unc-38(x20) I.*
RF566	*unc-38; mir-240/786*	*unc-38(x20) I; mir-240/ 786 (n4541) X.*
RF524	*unc-38 lfe-2*	*unc-38(x20) lfe-2(sy326) I.*
RF525	*unc-38 lfe-2; mir-240/786*	*unc-38(x20) lfe-2(sy326) I; mir-240/786(n4541) X.*
RF623	calcium imaging	*pha-1(e2123ts) III; him-5(e1490) V; rnyEx109 [Pnhx-2::D3cpv +pha-1(+)].*
RF624	calcium imaging	*pha-1(e2123ts) III; him-5(e1490) V; mir-240/786(n4541) X; rnyEx109 [Pnhx-2::D3cpv +pha-1(+)].*
RF701	pH imaging	*pha-1(e2123ts) III; rnyEx006 [Pnhx-2::pHluorin, pha1(+)]*
RF702	pH imaging	*pha-1(e2123ts) III; mir-240/786 (n4541) X; rnyEx006 [Pnhx-2::pHluorin, pha-1(+)]*
RF729	*elo-2^{prom}::GFP::elo-2$^{3'UTR}$*	*xwEx143 [elo-2^{prom}::GFP::elo-2$^{3'UTR}$; pRF4].*
RF750	*elo-2^{prom}::GFP::elo-2$^{3'UTR}$*	*mir-240/786(n4541) X; xwEx143 [elo-2^{prom}::GFP::elo-2$^{3'UTR}$; pRF4].*
RF752	*elo-2^{prom}::GFP::elo-2$^{3'UTRmut}$*	*xwEx147 [elo-2^{prom}::GFP::elo-2$^{3'UTRmut}$; pRF4].*
RF760	*elo-2^{prom}::GFP::elo-2$^{3'UTRmut}$*	*mir-240/786(n4541) X; xwEx147 [elo-2^{prom}::GFP::elo-2$^{3'UTRmut}$; pRF4].*

Supplemental Experimental Procedures

Strain Construction

For strain construction with the *mir-240/786 (n4541)* allele, PCR was used to determine the genotype, as previously described [1]. *itr-1* and *lfe-2* alleles were followed using the Unc phenotype of the closely linked *unc-24(e138*) and *unc-38(x20*) alleles, respectively. For these strains, sequencing was performed to confirm the presence of the *itr-1* or *lfe-2* allele. *sy605* is a 951 bp deletion in *ipp-5* and most likely represents a complete null of *ipp-5* [2]. *sy605* was followed using PCR with the following primers to genotype: AA782 (gctattcgtttgtttgcggatag) and AA783 (gaattgagaaacgttcgaccac) primers were used to detect the wild-type and deletion allele while AA782 and AA784 (gactatgagacattgcgtgagttc) were used to detect the wild-type allele.

Microscopy

Confocal microscopy was performed using a Nikon A1R Microscope. Nomarski DIC and epifluorescence microscopy was performed using a Nikon 80i compound microscope equipped with a CoolSNAP HQ2 (Roper Scientific) camera. Images were captured using Nikon Elements software. To analyze the time between posterior body contractions and expulsion events, videos were collected using a Nikon SMZ-1500 stereomicroscope by capturing images at 10 frames/s for 10 minutes (n = 10 worms).

Calcium and pH Imaging

Calcium and pH imaging was performed as described Imaging was performed on a TE200U inverted microscope (Nikon) equipped with a Sensicam CCD camera (Cooke), a Polychrome IV monochrometer (TILL Photonics) and a Nikon 10x Plan Fluor air objective (0.45 NA) on live well-fed worms moving freely on NGM-agarose plates. The worms were kept in-frame by manual manipulation of the microscope stage. Data collection and analysis was performed using TILLvisION software (TILL Photonics) and Microsoft Excel. For generating ratio images, background images were obtained under identical acquisition parameters as defined in the experimental protocol (see below). These images were subtracted from the experimental images on a pixel-by-pixel basis. The resulting background-subtracted images were subject to thresholding where pixels of less than ~20% the average background value at either of the two wavelengths were set to zero, hence limiting the ratio map to areas of actual fluorescence. Generally, in the context of the rather large *C. elegans* intestine and the uniformly bright biosensors employed in this study, ratios derived numerically from the individual emissions were nearly identical to those extracted from the ratio maps themselves.

Calcium measurements: Strains expressing the dual emission D3cpV calcium sensor [3] were imaged using a CFP/YFP filter cube (Chroma) and an emissions beamsplitter (Optical Insights). 50 ms pulses of 435 λ excitation were applied at 2 Hz. The resulting 480/535 λ emissions were split onto opposite sides of the CCD and binned at 2x2. A FRET module in TILLvisION was used to extract wavelength-specific emission images for generating ratio maps.

pH measurements: Strains expressing the dual excitation pH sensitive ratiometric GFP variant pHluorin [4] were imaged using a pHluorin filter cube (Chroma). The biosensor was excited at 2 Hz using sequential 20 ms 410/470 λ excitation pulses and its emissions were collected at 535 λ emission with 2x2 binning. Dual excitation ratios were converted to pH units based upon an in situ high potassium-nigericin calibration [5].

RNAi by Feeding
All bacteria for RNAi experiments were isolated from the Ahringer RNAi library with the following exception: a fragment of *frl-1* was PCR amplified (primers-ctgaggtacctacgaaatgacacttctcggattgg and ctagccatggcctgcatctgtttctgaatagcttc) and cloned into Kpn-I and NcoI sites in the pPD129.36/L4440 plasmid. This *frl-1* RNAi plasmid was transformed into HT115 bacteria. Bacteria from overnight cultures was plated onto RNAi plates (NGM supplemented with 1mM ITPG and 100 mg/ml ampicillin) and stored at room temperature for 24 hours to allow for induction of dsRNA. Twenty or more embryos were cloned to RNAi plates and young adults were monitored for defecation approximately 60-70 hours later.

Construction of expression constructs and reporter transgenes
To generate deletions in *mir-240* and *mir-786*, the Quikchange II kit (Stratagene) was used with the *mir-240/786* rescue plasmid, pAAS109 [6], as a template (Agilent Technologies). Primers for *mir-240* (5'-gagactagaatgcttgaattgtactagcATagaaatacagttcac-3' and 5'-gtgaactgtatttctATgctagtacaattcaagcattctagtctc-3') and *mir-786* (5'-ggtatttacaaaaagacaaaattGCggtgatgaatctcatttttattg-3' and 5'-caataaaaaatgagattcatcaccGCaattttgtctttttgtaaatacc-3') were used to create plasmids missing the 22 nt *mir-240* sequence (pBK130) or the 22nt *mir-786* sequence (pBK131). A plasmid missing both the *mir-240* and *mir-786* sequences (pBK133) was generated using the above primers and pBK130 as a template. Sequencing was performed to verify the deletion. Arrays were generated by injection of a rescuing plasmid at 25ng/ul, the co-injection marker pPD158.87 at 25ng/ul and 1 kb ladder (Invitrogen) at 80ng/ul.

To generate the *elo-2*^{prom}*::gfp::elo-2*$^{3'UTR}$ reporter (pBK134), the predicted *elo-2* promoter (2.8kb upstream of the first exon) was amplified using PCR (5'-gtacgagctctgtgattacctgcaaatttccacga-3' and 5'-gatcggatccgaagccctgtgtaagaggcttgaaatcac-3') and cloned into a SmaI site immediately upstream of GFP(65C)-PEST in the pAF207 plasmid [7]. Next, the *elo-2* 3'UTR (247 bp) was amplified using PCR (5'-gtacgaattccgagtaaatagtgataagcaacacgc-3' and 5'-gtacgaattcataaacattgtgaaaacttcaaaaatttcttgc-3') and cloned into an EcoRI site immediately downstream of the GFP(65C)-PEST. To generate the *elo-2*^{prom}*::gfp::elo-2*$^{3'UTRmut}$ transgene, the Quikchange II kit was used to delete the predicted miR-786 binding site from the *elo-2* 3' UTR from pBK134 to generate pBK143. For this Quikchange reaction, the following primers were used: (5'-gtcttgtttttctgactcatcatttttcaactttagattaatttctttgttaaatttatttttcattg-3' and 5'-caatgaaaaataaatttaacaaagaaattaatctaaagttgaaaaaatgatgagtcagaaaaacaagac-3'). Arrays were generated by injection of either pBK134 or pBK143 at 5ng/ul, with the co-injection marker pRF4 at 100ng/ul.

Fatty acid supplements: Palmitic acid sodium salt (Sigma) was dissolved in 1% NP-40 at 80°C and added to NGM agar plates containing ampicillin for a final concentration of 1.0mM. Plates were seeded with HT115 bacteria. Embryos were transferred to plates and were analyzed for defecation behavior as young adults. Worms grown on plates with 1% NP-40 were analyzed as a control.

qPCR
Total RNA was isolated using Trizol (Invitrogen). Reverse transcription was performed using iScript cDNA synthesis kit (Bio-Rad). Quantitative RT-PCR was performed with SYBR Green (Bio-Rad) and a CFX Connect detection system (Bio-Rad). Expression level of *elo-2* was normalized to the expression of *ama-1* and *pmp-3* {Hoogewijs et al., 2008, BMC Mol Biol, 9, 9}. The following primers were used for qPCR: *elo-2* (5'- tacgcagtagtcacatactctgagc-3' and 5'-

acggcgaagtagaaatacataacag-3'), *ama-1* (5'-cctacgatgtatcgaggcaaa-3' and 5'-cctccctccggtgtaataatg-3'), and *pmp-3* (5'-gttcccgtgttcatcactcat-3' and 5'-acaccgtcgagaagctgtaga-3'). qPCR reactions were performed in triplicate and qRT-PCR analysis was performed with two independent biological replicates.

Supplemental References

1. Brenner J.L., Jasiewicz K.L., Fahley A.F., Kemp B.J., and Abbott A.L. (2010). Loss of individual microRNAs causes mutant phenotypes in sensitized genetic backgrounds in C. elegans. Curr. Biol. *20*, 1321-1325.
2. Bui Y.K., and Sternberg P.W. (2002). Caenorhabditis elegans inositol 5-phosphatase homolog negatively regulates inositol 1,4,5-triphosphate signaling in ovulation. Mol. Biol. Cell *13*, 1641-1651.
3. Palmer A.E., Giacomello M., Kortemme T., Hires S.A., Lev-Ram V., Baker D., and Tsien R.Y. (2006). Ca2+ indicators based on computationally redesigned calmodulin-peptide pairs. Chem. Biol. *13*, 521-530.
4. Miesenböck G., De Angelis D.A., and Rothman J.E. (1998). Visualizing secretion and synaptic transmission with pH-sensitive green fluorescent proteins. Nature *394*, 192-195.
5. Thomas J.A., Buchsbaum R.N., Zimniak A., and Racker E. (1979). Intracellular pH measurements in Ehrlich ascites tumor cells utilizing spectroscopic probes generated in situ. Biochem. *18*, 2210-2218.
6. Miska E.A., Alvarez-Saavedra E., Abbott A.L., Lau N.C., Hellman A.B., McGonagle S.M., Bartel D.P., Ambros V.R., and Horvitz H.R. (2007). Most Caenorhabditis elegans microRNAs are individually not essential for development or viability. PLoS Genet. *3*, e215.
7. Frand A.R., Russel S., and Ruvkun G. (2005). Functional genomic analysis of C. elegans molting. PLoS Biol. *3*, e312.

Supplemental Movie S1

Click here to download Supplemental Movie and Spreadsheet: Movie S1.mp4

Supplemental Movie S2

Click here to download Supplemental Movie and Spreadsheet: Movie S2.mp4